Cell

Immuno- and Constitutive Proteasome Crystal Structures Reveal Differences in Substrate and Inhibitor Specificity

Eva M. Huber,[1,5] Michael Basler,[2,3,5] Ricarda Schwab,[2,5] Wolfgang Heinemeyer,[1] Christopher J. Kirk,[4] Marcus Groettrup,[2,3,*] and Michael Groll[1,*]

[1]Center for Integrated Protein Science at the Department Chemie, Lehrstuhl für Biochemie, Technische Universität München, Garching D-85747, Germany

[2]Division of Immunology, Department of Biology, University of Constance, Konstanz D-78457, Germany

[3]Biotechnology Institute Thurgau at the University of Constance, CH-8280 Kreuzlingen, Switzerland

[4]Onyx Pharmaceuticals, South San Francisco, CA 94080, USA

[5]These authors contributed equally to this work

*Correspondence: marcus.groettrup@uni-konstanz.de (M.G.), michael.groll@ch.tum.de (M.G.)

DOI 10.1016/j.cell.2011.12.030

SUMMARY

Constitutive proteasomes and immunoproteasomes shape the peptide repertoire presented by major histocompatibility complex class I (MHC-I) molecules by harboring different sets of catalytically active subunits. Here, we present the crystal structures of constitutive proteasomes and immunoproteasomes from mouse in the presence and absence of the epoxyketone inhibitor PR-957 (ONX 0914) at 2.9 Å resolution. Based on our X-ray data, we propose a unique catalytic feature for the immunoproteasome subunit β5i/LMP7. Comparison of ligand-free and ligand-bound proteasomes reveals conformational changes in the S1 pocket of β5c/X but not β5i, thereby explaining the selectivity of PR-957 for β5i. Time-resolved structures of yeast proteasome:PR-957 complexes indicate that ligand docking to the active site occurs only via the reactive head group and the P1 side chain. Together, our results support structure-guided design of inhibitory lead structures selective for immunoproteasomes that are linked to cytokine production and diseases like cancer and autoimmune disorders.

INTRODUCTION

Nucleated cells of most vertebrates utilize MHC-I molecules to present peptides to the cell surface. These peptides may be derived from intracellular self-proteins or have foreign viral or bacterial origin, but all are products of protein degradation by the 20S proteasome core particle (CP) (Grant et al., 1995; Hershko and Ciechanover, 1998; Michalek et al., 1993; Townsend et al., 1988). When a cytotoxic T cell binds to an immunogenic foreign peptide, embedded in the groove of MHC-I molecules, it is activated to kill the infected antigen-presenting cell (Rock and Goldberg, 1999). The T cell subsequently releases cytokines, particularly tumor necrosis factor-α and interferon-γ, that induce the expression of three specialized, catalytically active proteasomal β-subunits, designated β1i/LMP2, β2i/MECL-1, and β5i/LMP7 (Aki et al., 1994; Brown et al., 1991; Glynne et al., 1991; Groettrup et al., 1996; Kelly et al., 1991; Martinez and Monaco, 1991; Nandi et al., 1996). These immunoproteasome subunits (i-subunits) cooperatively assemble into nascent CPs, effectively substituting their constitutive counterparts (c-subunits) β1c/Y, β2c/Z, and β5c/X, respectively. Consequently, the de novo synthesis of CPs in inflamed tissues is largely in the form of immunoproteasomes (iCPs) (Griffin et al., 1998; Kingsbury et al., 2000). Whereas iCP expression is inducible in most tissues, it is constitutive in hematopoetic cells, especially lymphocytes and monocytes. Moreover, in cortical thymic epithelial cells, a third class of mammalian proteasome, the so-called thymoproteasome (tCP), is expressed, which bears the subunit β5t and is involved in the positive selection of developing T cells (Murata et al., 2007).

As a result of their different subunit compositions, constitutive proteasomes (cCPs), iCPs, and tCPs are endowed with different cleavage specificities; for example, iCPs preferentially hydrolyze proteins after nonpolar amino acids (Gaczynska et al., 1994). The peptides produced by iCPs further stimulate the immune system, as their hydrophobic C termini are perfect anchor motifs for binding to MHC-I molecules (Romero et al., 1991). However, it has been shown in gene-targeted mice that the i-subunits are not essential for epitope presentation in general, implying that the cCP is also to a considerable extent competent in antigen processing (Van den Eynde and Morel, 2001; Yewdell et al., 1994).

Recent studies reported that β5i plays a pivotal role in cytokine production, and that small-molecule inhibitors of this subunit have therapeutic activity in mouse models of autoimmune diseases and inflammatory disorders (Basler et al., 2010; Ichikawa et al., 2011; Muchamuel et al., 2009). Thus, selective inhibition of the iCP subunit β5i represents a promising therapeutic alternative to the approved proteasome inhibitor bortezomib,

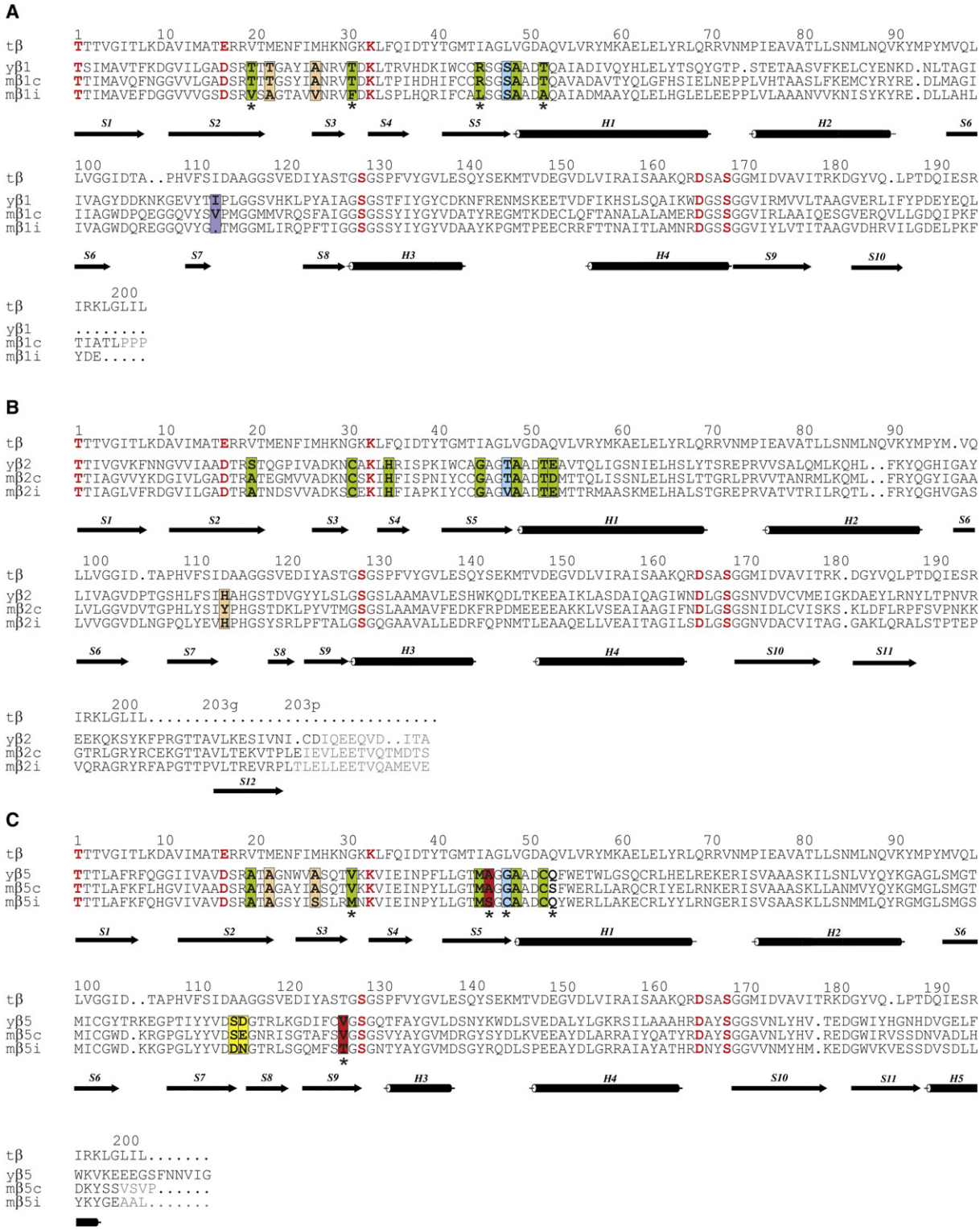

Figure 1. Sequence Alignments of the Catalytic β-Subunits from *T. acidophilum* and Yeast with Their Murine i- and c-Analogs

Residue numbers are assigned according to the sequence alignment to the β-subunit of *T. acidophilum*. Amino acid insertions compared to the sequence of *T. acidophilum* are designated by additional lowercase letters. Secondary structures (S: β sheet; H: helix) are indicated for the i-subunits. Structurally distorted amino acids are shown in gray, whereas residues important for the active site are displayed in red. Residues contributing to the substrate-specificity pockets are highlighted by colored boxes: S1 pocket, green; S2 pocket, blue; S3 pocket, brown; S′, yellow. Amino acid 113 is absent in all β1i-subunits (purple box). The

which often causes neurotoxicity (Badros et al., 2007). Currently, the irreversibly acting epoxyketone PR-957 is the most potent β5i-selective inhibitor (Muchamuel et al., 2009), but the molecular basis for its selectivity has remained elusive up to now.

Here, we examine the murine cCP and iCP at the molecular level and provide structural explanations for the enhanced MHC-I antigen generation by iCPs. Moreover, X-ray structures of the mouse cCP and iCP as well as the CP from *Saccharomyces cerevisiae* (yCP) in the presence and absence of PR-957 (ONX 0914) revealed the basis for the β5i selectivity of this compound.

RESULTS

Elucidation of iCP, cCP, and yCP Crystal Structures in Complex with PR-957

Preparations of iCPs were isolated from livers of BALB/c mice 8 days after infection with lymphocytic choriomeningitis virus (LCMV), and cCPs were purified from livers of uninfected $\beta2i^{-/-}$ $\beta5i^{-/-}$ gene-targeted mice (Khan et al., 2001; Schmidtke et al., 2000). After assessment of their purity by two-dimensional gel electrophoresis (Figure S1 available online), both proteins were crystallized from conditions containing 2,4-methyl-pentanediol (MPD). Diffraction data of native crystals and crystals soaked with the epoxyketone inhibitor PR-957 were recorded to a maximum resolution of 2.9 Å. Data evaluation with the coordinates of the bovine cCP (Protein Data Bank [PDB] ID 1IRU; Unno et al., 2002) was followed by positional refinement as well as model building using 4-fold and 2-fold noncrystallographic symmetry (NCS) averaging for cCP and iCP, respectively. Electron density maps proved that each subunit was well defined and that all catalytically active sites of both cCP and iCP showed full occupancy of PR-957. Positive and negative F_o-F_c maps clearly depicted expected sequence changes from c- to i-subunits, allowing us to assign amino acid side chains unambiguously (Figure 2). Residue numbers were allocated on the basis of the alignment to the β-subunit of *Thermoplasma acidophilum* (Figure 1 and Data S1) (Löwe et al., 1995). All models were completed with final R_{free} values below 27.5% and root-mean-square deviation (rmsd) bond and angle values of lower than 0.005 Å and 0.93° (Table S1).

To explore the docking and the two-step reaction mechanism of epoxyketones, yCP crystals were soaked with two different concentrations of PR-957, and X-ray data were evaluated as previously reported (Groll and Huber, 2005) (Table S2).

Architecture of the iCP

The quaternary structures of the cCP and iCP differ only in the substitution of the c-subunits β1c, β2c, and β5c by their i-counterparts β1i, β2i, and β5i (Figure 3A). The entry gates to the central proteolytic chambers are closed by the N termini of the α-subunits, and superposition of the α-rings from cCP and iCP reveals high structural similarity (rmsd $C_{\alpha\text{-rings}} < 0.59$ Å) (Figure S2). Thus, we speculate that regulation of the gating mechanism by activator complexes such as 19S, 11S (PA28), and PA200 is similar in cCPs and iCPs.

Structural superposition of identical α-subunits and inactive β-subunits from both proteasome types shows an rmsd of <0.35 Å for the C_α backbone. Remarkably, the main chain tracings of exchangeable c- and i-β-subunits also match almost perfectly (rmsd < 0.72 Å) (Figure 3B), despite the differences in their primary structures (sequence identity of β1c/β1i: 63.3%; β2c/β2i: 58.9%; β5c/β5i: 72.4%).

Most amino acid substitutions between murine c- and i-subunits are surface exposed, and comparison of the primary sequences of all known c- and i-subunits reveals that only a few substitutions occur in all species (β1i: 13.6%; β2i: 5.1%; β5i: 9.8%; Data S1B, S1D, and S1F). Moreover, the number of interactions that create contact surfaces between neighboring subunits varies from cCP to iCP (Table S3), but their influence on the overall stability of the complexes cannot be clarified from a structural point of view.

Insights into the Substrate-Binding Channels of the c- and i-Subunits

Substrate affinities toward proteasome active sites are solely determined by enthalpic interactions with the primed and unprimed substrate-binding channels (Figure 3C). Whereas subunits β2i and β2c are identical with respect to their primed pockets, subunit β1i is shortened by one residue in the region 113–124 compared to β1c (Figure 2A). This deletion is consistent among all β1i-subunits sequenced thus far and represents a hallmark feature that changes the possible contact sites for bound substrates. Similarly, the substitutions S115D and E116N in subunit β5i may affect cleavage preferences, but these residues are not conserved among species.

Compared to the primed pockets, the unprimed substrate-binding channels are far better characterized and can be subdivided in S1, S2, and S3 specificity sites (Figure 3C). Subunit β2i is the only i-subunit that is not encoded on the MHC cluster; interestingly, its substrate-binding channel was found to be identical with that of β2c, except for the substitution of Asp53 (β2c) with Glu (β2i). Furthermore, no differences were observed in the ligand-free and ligand-bound states (Figures S3A–S3D). Thus, the rationale for the incorporation of subunit β2i into the iCP remains elusive, and β2-subunits may play an additional functional role that has yet to be described.

In contrast to the consistent character of subunits β2c and β2i, several important distinctions were observed upon comparison of β1c and β1i. The conserved substitutions T20V, T31F, R45L, and T52A in β1i increase the hydrophobicity of the S1 pocket and diminish it in size (Figure S3E).

strictly conserved amino acid exchanges A46S and V127T in β5i, suggested to modulate the active site characteristics, are indicated by red boxes. Stars mark point mutations occupying prominent positions in the substrate-binding channel or near the active site.

(A) The β-subunit of *T. acidophilum* (tβ) is aligned with the β1-subunits from *S. cerevisiae* (yβ1) and *M. musculus* (mβ1c; mβ1i).

(B) Alignment of β2-subunits according to (A).

(C) Alignment of β5-subunits according to (A).

See also Data S1.

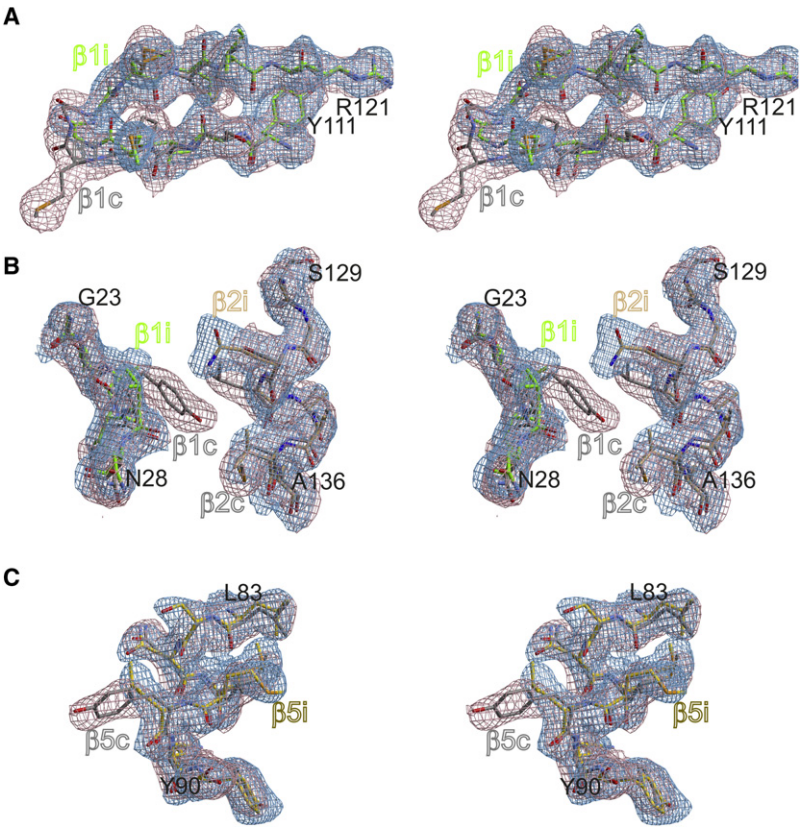

Figure 2. Stereo Representation of the Electron Density of Characteristic Segments of the Murine c- and i-β-subunits

The electron densities (i-subunits: blue; c-subunits: red) represent $2F_o$-F_c maps, with the displayed amino acids omitted for phasing. Contouring at even 0.8 σ clearly depicts prominent amino acid exchanges, excluding a mixture of cCPs and iCPs. Predominantly, exchanges of bulky residues in the cCP by smaller side chains in the iCP are shown.

(A) Superposition of the murine subunits β1i (green) and β1c (gray). The lack of amino acid 113 in the β1i-subunit results in shortening of the loop segment between Tyr111 and Arg121.

(B) Superposition of the interface of subunits β2i/β1i and β2c/β1c analogous to (A). The electron density shows amino acid exchanges, namely Y25A in subunit β1i (green) and S131Q, L132G, as well as M135V in subunit β2i (brown).

(C) Superposition of the murine subunits β5i (yellow) and β5c (gray) visualizes that Tyr88 is replaced by Leu in β5i. See also Figure S1.

Consequently, peptide bond hydrolysis preferentially occurs after small, hydrophobic, and branched residues and more epitopes with nonpolar C termini, such as Ile, Leu, or Val, are generated for the presentation on MHC-I molecules (Cardozo and Kohanski, 1998; Orlowski et al., 1993; Romero et al., 1991). This agrees with the specific cleavage of the fluorogenic model substrate Ac-PAL-AMC (Acetate-Pro-Ala-Leu-7-amino-methylcoumarin) by β1i (Blackburn et al., 2010). Apart from the S1 pocket, the amino acid substitutions T22A and A27V in β1i, as well as Y114H in the adjacent β2i-subunit, collectively shape, downsize, and polarize the S3 site of the β1i entity (Figure S3E).

In the S1 pockets of the subunits β5c and β5i, the residues that give rise to chymotrypsin-like (ChTL) activity, Ala20, Met45, Ala49, and Cys52, are unchanged. Only amino acid 31 is variable in size but conserved in its hydrophobic character (Figure S3I and Data S1F). In contrast to β5c-subunits, all known β5i entities harbor a shallow S2 pocket in position 48 formed by Cys or Ser. The substitution of Ala27 (β5c) by Ser (β5i) restricts the size of the S3 pocket of murine and human β5i and endows it with a more hydrophilic character compared to subunit β5c (Figure S3I).

In addition to these amino acid changes, the S1 pockets of β5c and β5i vary in their size. Distinct conformations of Met45 result in a spacious S1 pocket in β5i and a significantly smaller one in β5c (Figure S3I). Formation of a large S1 pocket, similar to chymotrypsin, is favored by strong van der Waals interactions of Met45 with the aliphatic side chain of Gln53. Whereas Gln53 is conserved in β5i-subunits, it is replaced in β5c-subunits by Ser, which cannot stabilize Met45 by hydrophobic interactions. As a result, β5c harbors a much smaller S1 pocket and thereby resembles elastase-like activity rather than ChTL activity. In addition, residue Lys32 (β5c)/Asn32 (β5i) may also be crucial for the distinct architecture of the S1 pocket in β5c and β5i.

Although the yCP contains Gln53 in yβ5, its interaction with Met45 is less dominant than in β5i; hence, Met45 adopts the same conformation as observed in β5c. From a structural perspective, yβ5 represents a chimera between β5c and β5i, as for example Lys32 is conserved in β5c-subunits and Gln53 in β5i entities.

Unique Active Site Architecture of Subunit β5i

The hydrophilicity surrounding the active site nucleophilic Thr1O$^{\gamma}$ and the oxyanion hole of subunit β5i is increased by the strictly conserved amino acid exchanges A46S and V127T. This elevated polarity might favor peptide bond hydrolysis by attracting water molecules. Moreover, the electron density displays a unique hydrogen bond network involving Gly47NH, as well as Ser46O$^{\gamma}$ and Thr127O$^{\gamma}$ (Figures 4C, 4E, and S3I). Because Ser46O$^{\gamma}$ is directly hydrogen bridged to the oxyanion hole Gly47NH (3.1 Å), it may contribute to the stabilization of the tetrahedral transition state during catalysis. This molecular feature is unique to β5i and could kinetically favor its proteolytic activity.

Molecular Basis for the Selectivity of PR-957 for Subunit β5i

In contrast to prominent proteasome inhibitors such as bortezomib, approved for the treatment of multiple myeloma and

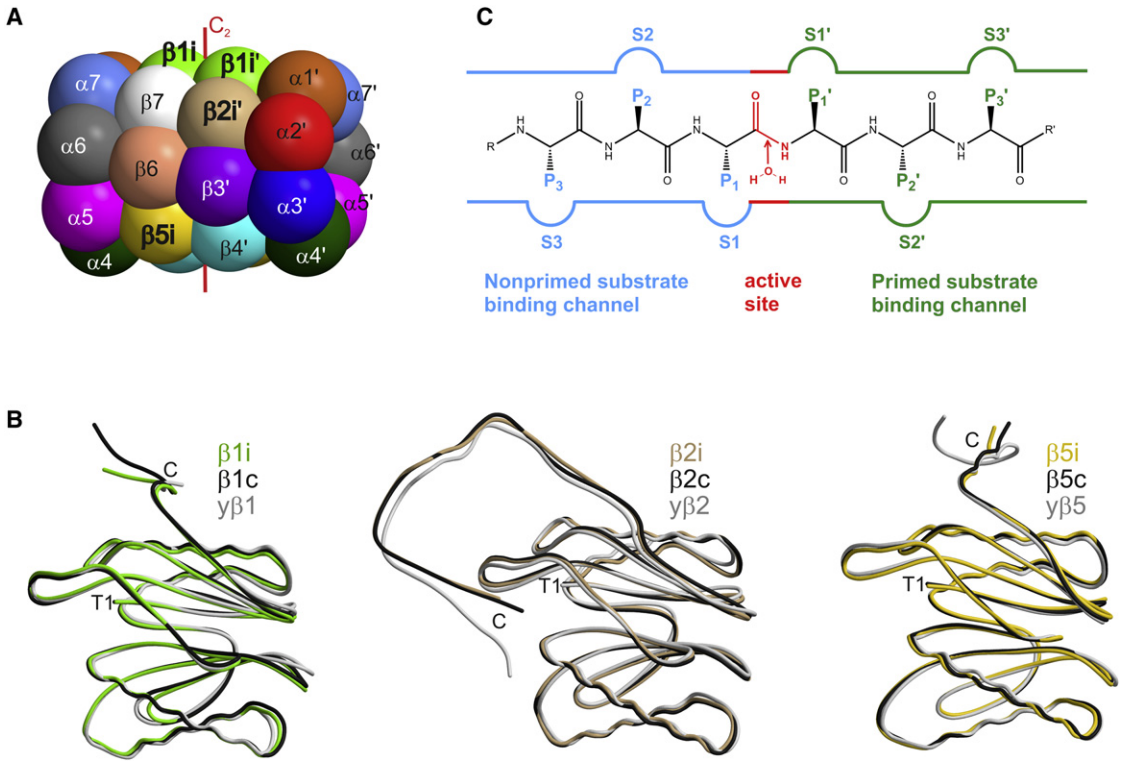

Figure 3. Topology of the Murine iCP

(A) Quaternary structure of the iCP drawn as spheres.

(B) Superposition of the C_α chain tracings of β1i (green), β2i (brown), and β5i (yellow) with their constitutive murine (black) and yeast (gray) counterparts, respectively. N and C termini as well as the nucleophilic Thr1 are labeled.

(C) Illustration of the substrate-specificity pockets of the three proteasomal activities and the S/P nomenclature of ligands. The unprimed (S) pockets, located N-terminally of the scissile peptide bond (red), and the corresponding substrate residues (P) are colored in blue. The primed (S′) pockets and the respective parts of the ligand (P′) are highlighted in green. The active site and the nucleophilic water molecule that is incorporated into the cleavage products during hydrolysis are shown in red.

See also Figure S2.

equally targeting the active sites of both β5c and β5i, PR-957 preferentially inhibits subunit β5i of iCPs (Muchamuel et al., 2009) (Figures 4A, 5, and S4). However, elucidation of the molecular basis for the selectivity of PR-957 requires the structural comparison of its binding to all active c- and i-subunits. Using inhibitor concentrations in the mM range for crystal soaking experiments, PR-957 targeted all active sites of the iCP and cCP (Muchamuel et al., 2009) as well as yCP and, by covalently binding in each case, proved that all three distinct catalytic centers are active in the crystals. Notably, although subunit β7 was suggested to harbor an active site in the bovine cCP apo-crystal structure (Unno et al., 2002), it was not occupied by PR-957 in the cCP and iCP.

The electron density maps display that the C-terminal dipeptide of PR-957 forms an antiparallel β sheet in each substrate-binding channel (Figure 4B), whereas the N-terminal morpholine moiety is not engaged in any interactions with the protein (Figures S5A–S5I). In all β2- and β5-subunits, the N-terminal peptide bond of the inhibitor is further stabilized by a hydrogen bond involving residue Asp114 of subunits β3 and β6 (Figures S5A–S5C and S5G–S5I).

All β2-subunits harbor very spacious S1 pockets that cannot sufficiently stabilize PR-957 in the substrate-binding channel and disfavor ligand binding compared to β5i for energetic reasons (Figures S3A–S3D and S5A–S5C). In contrast, binding of PR-957 to β1c is hampered due to steric hindrance by Arg45, which has to be dislocated to enable covalent modification of Thr1. Additionally, the hydrophilic S1 pocket of subunit β1c opposes binding of the hydrophobic P1 residue of PR-957. Although the hydrophobicity of the substrate-specificity pockets of β1i supports PR-957 binding, atomic distances indicate that Phe31 creates a steric barrier to the P1 phenyl moiety of PR-957 (Figures S3E–S3H and S5D–S5F). Hence, the inhibitor might bind only against significant repulsive forces mirrored in an unfavorable orientation of Phe31 toward the carbonyl oxygen of Asp32 (β1i).

To complement the crystal structures, the IC_{50} values of PR-957 for the ChTL activity of various CPs were determined (Figure 5). Inhibitory activity against murine, human, and yeast β5c-subunits was observed in the micromolar range (IC_{50} for mβ5c: 0.92 μM; hβ5c: 1.0 μM; yβ5: 0.55 μM). In contrast, β5i from mice and humans displayed IC_{50} values in the nanomolar

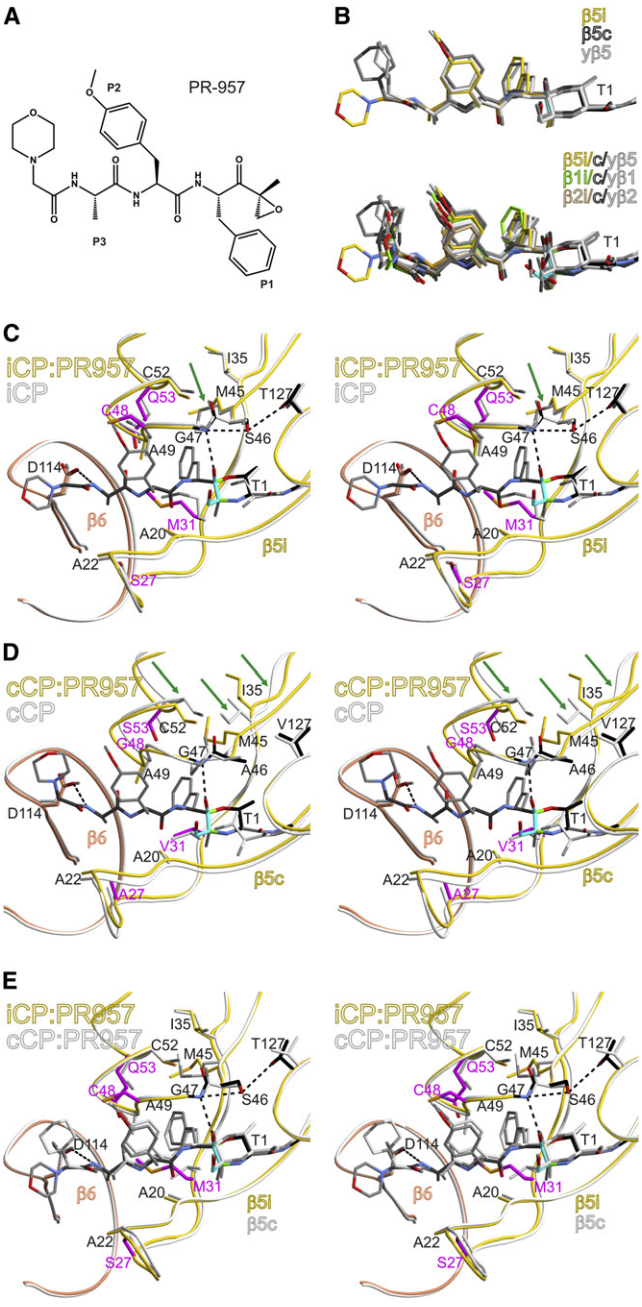

Figure 4. Structural Basis for the Selective Inhibition of iCPs by PR-957

(A) Chemical structure of PR-957.

(B) PR-957 molecules bound to β5i, β5c, and yβ5 are structurally superimposed in the upper panel. The lower panel illustrates the superposition of all PR-957 molecules bound to yCP, cCP, and iCP, revealing a common binding mode for the inhibitor backbone. The Thr1 residue is labeled.

(C) Structural superposition of murine subunit β5i alone (gray) and in complex with PR-957 (yellow) in stereo. Residues Thr1, Gly47, Ser46, and Thr127 are colored in black; amino acid exchanges apart from A46S and V127T compared to subunit β5c are highlighted in magenta. The epoxyketone moiety of PR-957 is marked in cyan and its peptidic backbone in gray. Hydrogen bonds are indicated by black dashed lines. Reorientation of the CH_3-S- group of Met45 upon ligand binding is indicated by a green arrow.

(D) Major structural changes in the substrate pockets of subunit β5c upon PR-957 binding are shown in stereo and marked by green arrows. Residues corresponding to the highlighted ones in (C) are color-coded according to (C).

(E) Comparison of the substrate-binding channels of β5i (yellow) and β5c (gray) after PR-957 binding in stereo representation. Colors are assigned according to (C) and (D).

See also Figure S3.

range, in agreement with previous studies (mβ5i: 65 nM; hβ5i: 73 nM) (Muchamuel et al., 2009).

To investigate this phenomenon, β5i-subunits were compared in the ligand-free and ligand-bound states, showing almost identical substrate-binding channels. Only minor structural reorientations of the CH_3-S- group of Met45, forming the bottom of the S1-specificity pocket, and Met31 are required to avoid clashing with the P1 phenylalanine of PR-957 (rmsd C_α β5i/β5i:PR-957: 0.28 Å) (Figures 4C, 6A, and 6B). However, superposition of β5c alone and in complex with PR-957 reveals that rotation of the whole side chain of Met45 is required for binding of PR-957 (Figures 4D, 6C, and 6D). This structural rearrangement in the S1-specificity pocket causes the reorientation of Ile35 and triggers further major conformational changes involving residues 34 to 76. Thus, PR-957 binding to the cCP results in the offset of the β sheets S4 and S5 as well as α helix H1 by up to 1.7 Å (rmsd C_α β5c/β5c:PR-957: 0.64 Å). Although superposition of the ligand-bound subunits β5c and β5i indicates structural similarity (rmsd C_α β5c:PR-957/β5i:PR-957: 0.55 Å) (Figures 4E, 6B, and 6D), covalent modification of β5c is hampered by steric hindrance with Met45, thereby explaining the selectivity of PR-957 for the ChTL activity of the iCP.

Due to comparable sizes of the S1 pockets of β5c and yβ5, binding of PR-957 to yβ5 is also hindered by Met45 and requires its dislocation (Figures 7D and S6D). Nevertheless, the IC_{50} value of PR-957 for subunit yβ5 is lower than for β5c (Figure 5), supporting the assumption that yβ5 may represent an intermediate stage between β5c and β5i.

Docking of PR-957 to the Active Site Thr1

Epoxyketones such as the natural product epoxomicin and its structural analog PR-957 have been proposed to react in a two-step mechanism with the N-terminal Thr1 of catalytically active proteasome subunits (Groll et al., 2000). To analyze the docking of the compound to the active site and to prove the order of reaction steps, we determined the crystal structures of yCPs incubated for varying times with different concentrations of PR-957. We obtained two datasets that clearly capture distinct reaction states of PR-957 with Thr1O^γ of yβ5 (Figures 7A and 7B) and that confirm the formerly proposed mode of action of epoxyketone inhibitors (Figure 7C). Following a reversible hemiketal formation of Thr1O^γ with the ketone group of PR-957 (Figures 7A and 7C), the epoxide is nucleophilically attacked by the amine group of Thr1, leading to the formation of a morpholine ring by an irreversible intermolecular cyclization (Figures 7B and 7C).

Remarkably, in the electron density map representing the hemiketal formation, the intact epoxide of PR-957 and only its P1 site are structurally defined (Figure 7A). Even though the P1

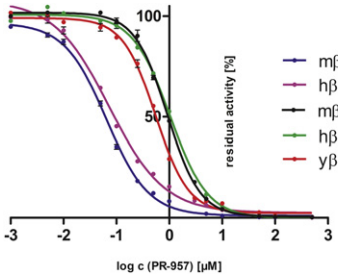

β5-subunit	IC_{50} [μM]
mβ5i	0.065 ± 0.005
hβ5i	0.073 ± 0.011
mβ5c	0.917 ± 0.054
hβ5c	1.036 ± 0.054
yβ5	0.551 ± 0.035

Figure 5. Inhibitory Potency of PR-957 for β5-Subunits of Various CPs

Yeast CP, mouse cCP and iCP, as well as human cCP and iCP were incubated with varying concentrations of PR-957 (0.001–500 μM). Data from three individual experiments were normalized to dimethylsulfoxide (DMSO) treated controls and are presented as relative activity ± standard deviation. IC_{50} values are given.

See also Figure S4.

site is not yet properly positioned, as indicated by superposition with the fully reacted PR-957 (Figure 7E), the first docking of the inhibitor to the active site occurs solely by its reactive functional group and its interactions with the S1 pocket of the active β-subunit. Subsequent contacts with the S2 and S3 sites lead to the formation of an antiparallel β sheet of the peptide moiety in the substrate-binding channel. Despite the importance of all three substrate-specificity pockets for the selectivity of a compound and for its IC_{50} value, our complex structures provide evidence that predominantly differences in the S1-binding pocket, in particular the orientation of Met45, are largely responsible for the enhanced affinity of PR-957 for β5i compared to β5c.

DISCUSSION

Our crystallographic data on the cCP and iCP reveal a similar architecture for c- and i-subunits, which is expected from an evolutionary point of view. However, our findings highlight the influence of subtle, yet biologically significant changes that could not have been predicted based on the existing structures of the yCP and bovine cCP. The differences in c- and i-subunits provide an explanation for enhanced antigen processing by iCPs as well as the molecular basis for the β5i selectivity of the inhibitor PR-957 and could be elucidated only by comparison of the six crystal structures reported in this work.

Molecular Differences between the c- and i-Subunits and Their Implications for Antigen Processing

Due to their high structural similarity, both β2c and β2i are able to generate MHC-I epitopes with neutral or basic C-terminal anchor residues (Rammensee et al., 1995). In addition, as often suggested, the structure of the iCP proves that the β1i substrate-binding channel is lined with hydrophobic amino acids, which enhance the production of MHC-I epitopes ending with small, nonpolar residues (Boes et al., 1994; Groll et al., 1997; Orlowski et al., 1993). Thus, in β1i-deficient mice, the peptide specificity of cytotoxic T cell responses is altered (Chen et al., 2001).

Apart from β1i, subunit β5i also enhances the generation of MHC-I ligands (Gaczynska et al., 1994). Our data suggest that peptide bond hydrolysis might be favored by an increased hydrophilicity of the active site and additional hydrogen bonds modulating the oxyanion hole. In particular, the presence of the strictly conserved residues Ser46 and Thr127 (Data S1F) might lead to a dominant active site in the iCP, which may explain the outstanding role of subunit β5i in antigen presentation. Indeed, increased processing kinetics were reported to stimulate the immunogenicity of antigens (Deol et al., 2007), and the activity of the 26S immunoproteasome was shown to be two times higher than that of its constitutive counterpart (Seifert et al., 2010).

In addition, compared to β5c, the introduction of an S2 pocket in subunit β5i augments its specificity for the P2 site of protein substrates and might influence its cleavage pattern.

However, most striking is the distinct conformation of Met45 in β5i relative to β5c, leading to differently sized S1 pockets. The smaller S1 pocket of β5c predominantly accommodates peptides with tiny hydrophobic amino acids such as Ala or Val. In contrast, the significantly enlarged S1 pocket of β5i leads to a preferential cleavage after large nonpolar residues like Tyr (Gaczynska et al., 1994), Trp, and Phe. These observations agree with the specific hydrolysis of the known fluorogenic substrates Ac-WLA-AMC and Ac-ANW-AMC by β5c and β5i, respectively (Blackburn et al., 2010).

Nonetheless, both ChTL activities display a certain degree of overlapping substrate specificities, especially with respect to Leu, Ile, and Tyr. Ligand docking to the active site reveals that Leu and Ile nicely fit into β5c; however, after initial binding to the S1 site, Met45 still must perform structural rearrangements (Figures 7E and S4B). Tyr also induces the dislocation of Met45, but its hydroxyl group can be stabilized in the S1 pocket by Ser53 of subunit β5c and Ser129 of the neighboring subunit β6.

In conclusion, β5i plays a key role in antigen processing by producing a broad variety of MHC-I epitopes ending with a branched or spacious hydrophobic anchor residue (Rammensee et al., 1995). In accord with our hypotheses, β5i- but not β1i- or β2i-deficient mice show a 50% reduced expression of MHC-I molecules (Basler et al., 2006; Fehling et al., 1994; Groettrup et al., 2010; Van Kaer et al., 1994) and are more susceptible to infectious diseases (Tu et al., 2009). Moreover, as subunit β5i is involved in cytokine production (Muchamuel et al., 2009), it may proteolytically activate certain regulatory factors by cleavage after bulky hydrophobic amino acid residues.

The importance of the ChTL activity for antigen presentation is further supported by recent studies on the tCP, which differs from the iCP only by the exchange of subunit β5i with β5t. Lining of the substrate-binding channel of β5t with the hydrophilic side chains Ser20, Ser31, Thr45, and Ser49 reduces the ChTL activity and leads to the production of low-affinity epitopes for MHC-I receptors (Data S1G). This might be crucial for the positive selection of developing T cells in the thymus (Murata et al., 2007; Tomaru et al., 2009; van Endert, 2011).

Based on the structural similarity of CPs, we attempted to investigate the subtle differences between the subunits β5c and β5i in more detail. By mutation of key amino acids in yβ5, we tried to mimic main characteristics of subunit β5i in yeast.

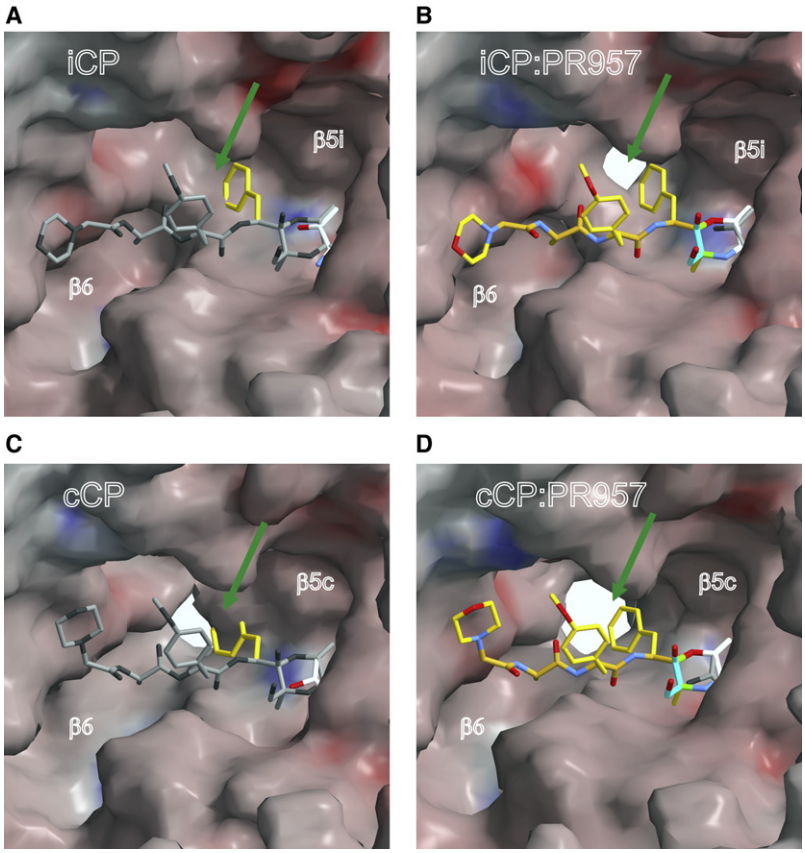

Figure 6. Conolly Surface Representation of the β5c and β5i Active Sites in the Presence and Absence of PR-957

Surface charge distributions are shown for the ChTL active sites of iCP (A), iCP:PR-957 (B), cCP (C), and cCP:PR-957 (D). Surface colors indicate positive and negative electrostatic potentials contoured from 50 kT/e (intense blue) to −50 kT/e (intense red). In order to illustrate conformational changes, the amino acids 46–50 were removed. Thr1 is colored in white, and the inhibitor PR-957, being part of the structures shown in (B) and (D), is highlighted in yellow. (A) and (C) display the PR-957 molecule of (B) and (D) modeled into the ligand-free substrate-binding channel by superposition of (A) and (B) as well as (C) and (D), respectively. Except for the P1 residue, the inhibitor is colored in gray in (A) and (C), as it does not belong to the displayed structure. Structural clashes and subsequent rearrangements are marked by green arrows.

(A) Illustration of the electrostatic potential of the ligand-free β5i substrate-binding channel. The green arrow marks the position where the phenyl side chain (yellow) of PR-957 would touch the CH_3-S- group of Met45 of subunit β5i.

(B) Conolly surface representation of subunit β5i in complex with PR-957. A steric clash with the phenyl side chain of the ligand (indicated in A by a green arrow) is prevented by reorientation of the CH_3-S- group of Met45 of subunit β5i (illustrated by the formation of a hole in the conolly surface and marked by a green arrow). See also Figure 4C.

(C) Illustration of the ligand-free β5c substrate-binding channel. Binding of PR-957 to β5c is hampered by severe clashes of the Phe side chain of PR-957 with Met45 of β5c (indicated by a green arrow).

(D) Insights into the ligand-bound β5c active site. Reaction of PR-957 with the nucleophilic Thr1 requires major structural rearrangements involving the complete side chain of Met45 (illustrated by the extension of the hole in the conolly surface and indicated by a green arrow). See also Figure 4D.
See also Figure S5.

However, thus far none of the mutants displays an affinity for PR-957 that is comparable to that of mammalian β5i (E.M.H., M. Groll, W.H., unpublished data). Additionally, exchange of yβ5 by the corresponding murine or human i-subunit was lethal to yeast, even after replacement of their genuine propeptides by that of yβ5. These observations might reflect the different assembly pathways of the yCP/cCP as well as iCP (Chen and Hochstrasser, 1996; De et al., 2003; Nandi et al., 1997) and the high phylogenetic distance between yeast and mouse. Furthermore, our structural data indicate that the amino acids in proximity to the active site and on the contact surfaces to adjacent subunits form a unique network that is specific for each organism and, thus, cannot be simply transferred between species.

Structural Requirements for Selective iCP Inhibitors

In autoimmune and neurodegenerative diseases, as well as in various types of cancer, the levels of proinflammatory cytokines are elevated resulting in increased iCP expression (Díaz-Hernández et al., 2003; Ho et al., 2007; Puttaparthi and Elliott, 2005; Singh et al., 2011; Visekruna et al., 2009). In several studies, the β5i-specific compound PR-957 has been shown to reduce the level of cytokines and autoantibodies, to modulate cytotoxic T cell responses, and to prevent disease progression in rheumatoid arthritis, experimental colitis, as well as systemic lupus erythematosus (Basler et al., 2010; Ichikawa et al., 2011; Muchamuel et al., 2009).

Our crystallographic investigations on PR-957 revealed a binding mechanism common to all active sites of cCP, iCP, and yCP (Figure 4B), and thus, its selectivity depends, apart from the reactive warhead, solely on the interactions with the substrate-binding channel. Furthermore, docking of PR-957 was shown to occur via its functional headgroup and the P1 site. This is consistent with the observation that nonpeptidic proteasome inhibitors such as salinosporamide A and omuralide target only the S1 pocket (Groll et al., 1997, 2006b). However, peptidic compounds like PR-957 form an antiparallel β sheet in the substrate-binding channel, indicating that the P2 and P3 sites also contribute to their specificity.

Based on the following structural requirements, inhibitors specific for β1c, β1i, β5c, or β5i can now be developed: the S1 pocket of subunit β1c favors negatively charged residues, whereas the corresponding pocket in β1i accommodates branched nonpolar side chains. Additionally, comparing subunits β1c and β1i, the latter prefers smaller and more polar amino acids in P3. β5c-selective compounds require hydrophobic residues like Leu or less structurally demanding amino

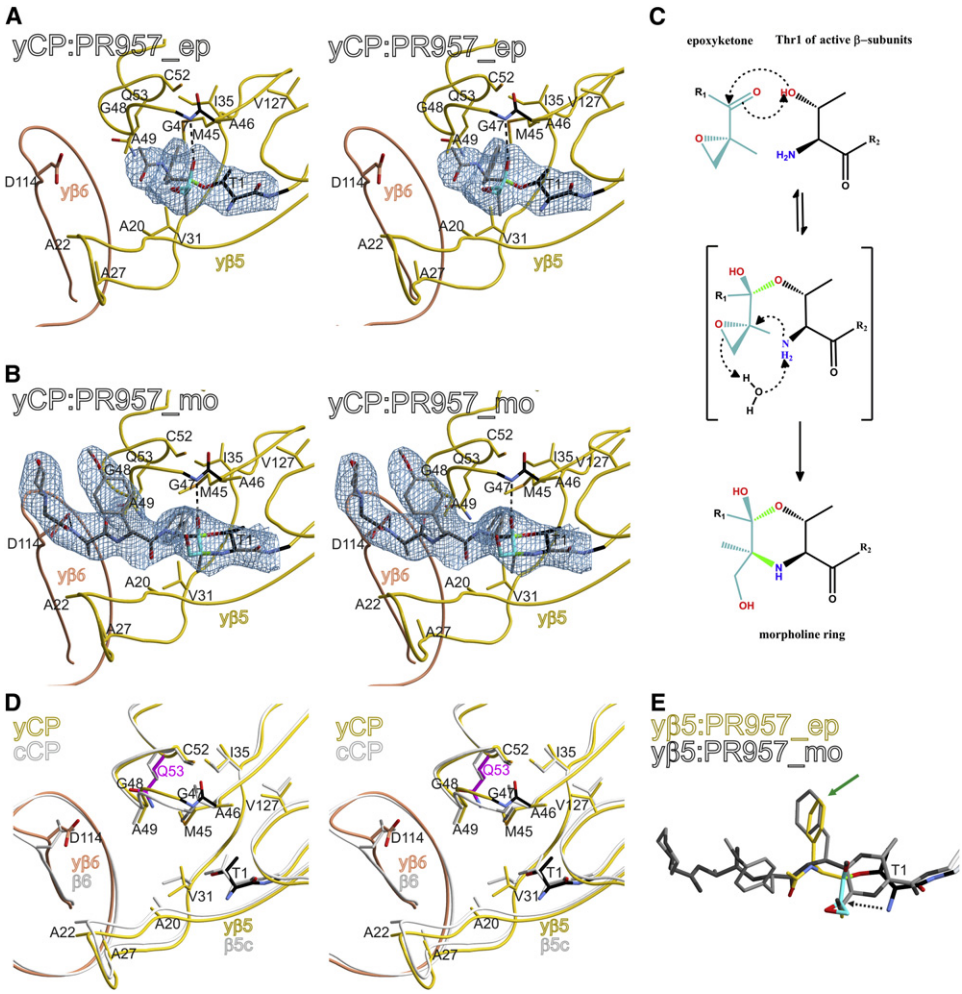

Figure 7. Probing the Docking and Reaction Mechanism of Epoxyketone Inhibitors

(A) Stereo representation of yβ5 in complex with partially reacted PR-957 still containing the intact epoxide group. Only the electrophilic head group and the P1 site of the partly reacted PR-957 are defined in the electron density. Residues Thr1 and Gly47 are colored in black. The epoxyketone moiety of PR-957 is marked in cyan, and its peptidic backbone in gray. Hydrogen bonds are indicated by black dashed lines. The $2F_o$-F_c electron density for the ligand is shown in blue and is contoured at 1 σ. The inhibitor and Thr1 have been omitted for phasing. Note that PR-957 in this structure was bound only to the ChTL active site of the yCP.

(B) Illustration of subunit yβ5 in complex with the fully reacted PR-957 according to (A). In contrast to the partially reacted PR-957 (A), the fully reacted inhibitor occupies all catalytically active sites (see Figures S5C and S5F, S5J–S5L, and S6).

(C) Schematic representation of the reaction mechanism of epoxyketone inhibitors. Reversible formation of a hemiketal by a nucleophilic attack of Thr1O^{γ} on the ketone group of the inhibitor is followed by an irreversible cyclization involving the N terminus of the proteasomal subunit and resulting in opening of the epoxide as well as generation of a morpholine ring. Bonds newly formed during this reaction are colored in green. R_1 designates the N-terminal part of the inhibitor, R_2 the active β-subunit.

(D) Superposition of the subunits yβ5 and β5c, pointing out the structural similarity of both CPs. The side chain Gln53 in yβ5, the only sequence difference in the S1 pocket compared to β5c, is marked in magenta. Gly47 and Thr1 are colored in black.

(E) Superposition of PR-957 in its epoxide (ep; yellow) and morpholine (mo; gray) form bound to subunit yβ5. Note that during docking, the P1 residue is not yet properly positioned in the S1 pocket (green arrow). A black dashed arrow marks the position where Thr1NH_2 attacks the intact epoxide group, resulting in the irreversible formation of a secondary amine as part of the morpholine ring.

See also Figure S6.

acids in P1 and bulky hydrophobic side chains in P3. In contrast, inhibitors specific for subunit β5i need large hydrophobic groups such as Trp or Phe in P1 (Toes et al., 2001) and small polar residues in P3.

The phenyl side chain of PR-957 perfectly fits into the spacious S1 pocket of β5i but not into the smaller one of β5c, which explains the subunit specificity of this inhibitor. The forces necessary to enlarge the S1 pocket of β5c by pushing Met45 aside are mirrored in the almost 15 times higher IC_{50} value of PR-957 for β5c. Similarly, engineered derivatives of omuralide and salinosporamide A, with a phenyl moiety in P1, have been demonstrated to exert significantly reduced

inhibitory potency toward the ChTL activity of yCP and cCP compared to the natural products (Corey and Li, 1999; Nett et al., 2009). Because salinosporamide A (marizomib) is tested in clinical phase studies (Potts et al., 2011), it would be interesting to characterize the selectivity of these derivatives for the iCP.

Besides PR-957, our structural data provide an explanation for the selectivity of well-characterized proteasome inhibitors (Figure S4A): As carfilzomib, currently in clinical phase 3 trials (Khan and Stewart, 2011), and PR-825 harbor Leu side chains in P1 and hydrophobic residues in P3, they both favor subunit β5c over β5i. Whereas the tripeptidic inhibitor PR-825 is >10-fold more selective for β5c, the tetrapeptide carfilzomib displays only slight specificity for β5c (<3-fold), indicating that P2, P3, and P4 residues also significantly influence the degree of selectivity (Kuhn et al., 2007; Muchamuel et al., 2009).

In contrast, bortezomib targets both ChTL activities to the same extent (Demo et al., 2007). Superposition of the murine CPs with the yCP:bortezomib X-ray structure (Groll et al., 2006a) reveals that the N-terminal pyrazole ring of bortezomib can occupy the S3 pocket of both β5c and β5i by interacting with Thr21, Ala22, and Ala27/Ser27 of β5c/i as well as Asp114 of β6 (Figure S4B). Based on our crystal structures and with respect to a sequence identity of more than 90% between murine and human proteasomal subunits, the selectivity of bortezomib could now be improved for either iCP or cCP.

In conclusion, the presented crystal structures of cCP and iCP from the same species enable molecular modeling studies with both mammalian proteasome classes for the first time. Using the outline above, it is now possible to undertake the structure-guided design of inhibitors that target single proteasomal subunits in order to modulate signaling processes such as antigen presentation or cytokine production, both of which play pivotal roles in various diseases. The ability to visualize the unique characteristics of iCP that evolved to serve immune responses may offer humankind a therapeutic window of opportunity.

EXPERIMENTAL PROCEDURES

Purification of CPs

Murine cCPs were purified from livers of $\beta2i^{-/-}$ and $\beta5i^{-/-}$ gene targeted mice as previously described (Schmidtke et al., 2000). To obtain iCP samples, BALB/c mice were infected intravenously with 200 p.f.u. LCMV-WE leading to an almost complete conversion to iCPs in the liver on day 8 post-infection (Khan et al., 2001), when organs were removed. Murine iCPs were purified from pooled livers (Schmidtke et al., 2000). Human cCPs were isolated from erythrocytes (Schmidtke et al., 2000), and human iCPs were purchased from Enzo Life Sciences. yCPs were isolated applying standard protocols (Groll and Huber, 2005).

Crystallization and Structure Determination of cCP and iCP

cCP and iCP crystals grew from a 1:1 mixture of protein (30 mg/ml) and reservoir solution (iCP: 0.2 M sodium iodide, 40% MPD; cCP: 0.2 M sodium formate, 40% MPD). cCP and iCP crystals were soaked with PR-957 at a final concentration of 3 mM for 8 hr. Structures were solved by molecular replacement using the bovine cCP as a starting model (PDB ID 1IRU) (Unno et al., 2002) and refined according to standard procedures (see Extended Experimental Procedures).

ACCESSION NUMBERS

Atomic coordinates have been deposited in the RCSB Protein Data Bank under the accession codes 3UNH (iCP), 3UNE (cCP), 3UNF (iCP:PR-957), 3UNB (cCP:PR-957), 3UN8 (yCP:PR-957_ep), and 3UN4 (yCP:PR-957_mo).

SUPPLEMENTAL INFORMATION

Supplemental Information includes Extended Experimental Procedures, six figures, a Data S1 file, and three tables and can be found with this article online at doi:10.1016/j.cell.2011.12.030.

ACKNOWLEDGMENTS

This work is dedicated to Professor Robert Huber on the occasion of his 75th birthday. We are grateful to B. Potts for fruitful discussions on the manuscript and to R. Huber for sharing his knowledge in the proteasome field with us. G. Werner, U. Beck, and the personnel of the animal research facility of Constance University are acknowledged for experimental support. We thank Richard Feicht for the purification of yCPs. The staff of the beamlines X06SA and X06DA at the Paul Scherrer Institute, SLS, Villigen, Switzerland, especially Takashi Tomizaki, is acknowledged for assistance during data collection. This work was supported by the Deutsche Forschungsgemeinschaft SFB595/TP A11 (M. Groll), BMBF-ProNET-T3 project To-03 (M. Groll), the Swiss National Fonds grant 31003A_138451 (M. Groettrup), and DFG grant 1517/12-1 (M. Groettrup, M.B.). R.S. is supported by the Graduate School of Chemical Biology at Constance University. M. Groll and M. Groettrup designed experiments. M.B. and R.S. purified cCPs and iCPs. E.M.H. performed activity tests and crystallographic experiments. W.H. and E.M.H. performed yeast genetics. C.J.K. provided PR-957 and edited the manuscript. E.M.H. and M. Groll collected and analyzed crystallographic data and wrote the manuscript. C.J.K. is an employee and stock holder of Onyx Pharmaceuticals.

Received: September 23, 2011
Revised: November 17, 2011
Accepted: December 2, 2011
Published: February 16, 2012

REFERENCES

Aki, M., Shimbara, N., Takashina, M., Akiyama, K., Kagawa, S., Tamura, T., Tanahashi, N., Yoshimura, T., Tanaka, K., and Ichihara, A. (1994). Interferon-gamma induces different subunit organizations and functional diversity of proteasomes. J. Biochem. *115*, 257–269.

Badros, A., Goloubeva, O., Dalal, J.S., Can, I., Thompson, J., Rapoport, A.P., Heyman, M., Akpek, G., and Fenton, R.G. (2007). Neurotoxicity of bortezomib therapy in multiple myeloma: a single-center experience and review of the literature. Cancer *110*, 1042–1049.

Basler, M., Moebius, J., Elenich, L., Groettrup, M., and Monaco, J.J. (2006). An altered T cell repertoire in MECL-1-deficient mice. J. Immunol. *176*, 6665–6672.

Basler, M., Dajee, M., Moll, C., Groettrup, M., and Kirk, C.J. (2010). Prevention of experimental colitis by a selective inhibitor of the immunoproteasome. J. Immunol. *185*, 634–641.

Blackburn, C., Gigstad, K.M., Hales, P., Garcia, K., Jones, M., Bruzzese, F.J., Barrett, C., Liu, J.X., Soucy, T.A., Sappal, D.S., et al. (2010). Characterization of a new series of non-covalent proteasome inhibitors with exquisite potency and selectivity for the 20S beta5-subunit. Biochem. J. *430*, 461–476.

Boes, B., Hengel, H., Ruppert, T., Multhaup, G., Koszinowski, U.H., and Kloetzel, P.M. (1994). Interferon gamma stimulation modulates the proteolytic activity and cleavage site preference of 20S mouse proteasomes. J. Exp. Med. *179*, 901–909.

Brown, M.G., Driscoll, J., and Monaco, J.J. (1991). Structural and serological similarity of MHC-linked LMP and proteasome (multicatalytic proteinase) complexes. Nature *353*, 355–357.

Cardozo, C., and Kohanski, R.A. (1998). Altered properties of the branched chain amino acid-preferring activity contribute to increased cleavages after branched chain residues by the "immunoproteasome". J. Biol. Chem. *273*, 16764–16770.

Chen, P., and Hochstrasser, M. (1996). Autocatalytic subunit processing couples active site formation in the 20S proteasome to completion of assembly. Cell *86*, 961–972.

Chen, W., Norbury, C.C., Cho, Y., Yewdell, J.W., and Bennink, J.R. (2001). Immunoproteasomes shape immunodominance hierarchies of antiviral CD8(+) T cells at the levels of T cell repertoire and presentation of viral antigens. J. Exp. Med. *193*, 1319–1326.

Corey, E.J., and Li, W.D. (1999). Total synthesis and biological activity of lactacystin, omuralide and analogs. Chem. Pharm. Bull. (Tokyo) *47*, 1–10.

De, M., Jayarapu, K., Elenich, L., Monaco, J.J., Colbert, R.A., and Griffin, T.A. (2003). Beta 2 subunit propeptides influence cooperative proteasome assembly. J. Biol. Chem. *278*, 6153–6159.

Demo, S.D., Kirk, C.J., Aujay, M.A., Buchholz, T.J., Dajee, M., Ho, M.N., Jiang, J., Laidig, G.J., Lewis, E.R., Parlati, F., et al. (2007). Antitumor activity of PR-171, a novel irreversible inhibitor of the proteasome. Cancer Res. *67*, 6383–6391.

Deol, P., Zaiss, D.M., Monaco, J.J., and Sijts, A.J. (2007). Rates of processing determine the immunogenicity of immunoproteasome-generated epitopes. J. Immunol. *178*, 7557–7562.

Díaz-Hernández, M., Hernández, F., Martín-Aparicio, E., Gómez-Ramos, P., Morán, M.A., Castaño, J.G., Ferrer, I., Avila, J., and Lucas, J.J. (2003). Neuronal induction of the immunoproteasome in Huntington's disease. J. Neurosci. *23*, 11653–11661.

Fehling, H.J., Swat, W., Laplace, C., Kühn, R., Rajewsky, K., Müller, U., and von Boehmer, H. (1994). MHC class I expression in mice lacking the proteasome subunit LMP-7. Science *265*, 1234–1237.

Gaczynska, M., Rock, K.L., Spies, T., and Goldberg, A.L. (1994). Peptidase activities of proteasomes are differentially regulated by the major histocompatibility complex-encoded genes for LMP2 and LMP7. Proc. Natl. Acad. Sci. USA *91*, 9213–9217.

Glynne, R., Powis, S.H., Beck, S., Kelly, A., Kerr, L.A., and Trowsdale, J. (1991). A proteasome-related gene between the two ABC transporter loci in the class II region of the human MHC. Nature *353*, 357–360.

Grant, E.P., Michalek, M.T., Goldberg, A.L., and Rock, K.L. (1995). Rate of antigen degradation by the ubiquitin-proteasome pathway influences MHC class I presentation. J. Immunol. *155*, 3750–3758.

Griffin, T.A., Nandi, D., Cruz, M., Fehling, H.J., Kaer, L.V., Monaco, J.J., and Colbert, R.A. (1998). Immunoproteasome assembly: cooperative incorporation of interferon gamma (IFN-gamma)-inducible subunits. J. Exp. Med. *187*, 97–104.

Groettrup, M., Kraft, R., Kostka, S., Standera, S., Stohwasser, R., and Kloetzel, P.M. (1996). A third interferon-gamma-induced subunit exchange in the 20S proteasome. Eur. J. Immunol. *26*, 863–869.

Groettrup, M., Kirk, C.J., and Basler, M. (2010). Proteasomes in immune cells: more than peptide producers? Nat. Rev. Immunol. *10*, 73–78.

Groll, M., and Huber, R. (2005). Purification, crystallization, and X-ray analysis of the yeast 20S proteasome. Methods Enzymol. *398*, 329–336.

Groll, M., Ditzel, L., Löwe, J., Stock, D., Bochtler, M., Bartunik, H.D., and Huber, R. (1997). Structure of 20S proteasome from yeast at 2.4 A resolution. Nature *386*, 463–471.

Groll, M., Berkers, C.R., Ploegh, H.L., and Ovaa, H. (2006a). Crystal structure of the boronic acid-based proteasome inhibitor bortezomib in complex with the yeast 20S proteasome. Structure *14*, 451–456.

Groll, M., Huber, R., and Potts, B.C. (2006b). Crystal structures of Salinosporamide A (NPI-0052) and B (NPI-0047) in complex with the 20S proteasome reveal important consequences of beta-lactone ring opening and a mechanism for irreversible binding. J. Am. Chem. Soc. *128*, 5136–5141.

Groll, M., Kim, K.B., Kairies, N., Huber, R., and Crews, C.M. (2000). Crystal structure of epoxomicin: 20S proteasome reveals a molecular basis for selectivity of α′, β′-epoxyketone proteasome inhibitors. J. Am. Chem. Soc. *122*, 1237–1238.

Hershko, A., and Ciechanover, A. (1998). The ubiquitin system. Annu. Rev. Biochem. *67*, 425–479.

Ho, Y.K., Bargagna-Mohan, P., Wehenkel, M., Mohan, R., and Kim, K.B. (2007). LMP2-specific inhibitors: chemical genetic tools for proteasome biology. Chem. Biol. *14*, 419–430.

Ichikawa, H.T., Conley, T., Muchamuel, T., Jiang, J., Lee, S., Owen, T., Barnard, J., Nevarez, S., Goldman, B.I., Kirk, C.J., et al. (2011). Novel proteasome inhibitors have a beneficial effect in murine lupus via the dual inhibition of type i interferon and autoantibody secreting cells. Arthritis Rheum. Published online September 8 2011. 10.1002/art.33333.

Kelly, A., Powis, S.H., Glynne, R., Radley, E., Beck, S., and Trowsdale, J. (1991). Second proteasome-related gene in the human MHC class II region. Nature *353*, 667–668.

Khan, M.L., and Stewart, A.K. (2011). Carfilzomib: a novel second-generation proteasome inhibitor. Future Oncol. *7*, 607–612.

Khan, S., van den Broek, M., Schwarz, K., de Giuli, R., Diener, P.A., and Groettrup, M. (2001). Immunoproteasomes largely replace constitutive proteasomes during an antiviral and antibacterial immune response in the liver. J. Immunol. *167*, 6859–6868.

Kingsbury, D.J., Griffin, T.A., and Colbert, R.A. (2000). Novel propeptide function in 20 S proteasome assembly influences beta subunit composition. J. Biol. Chem. *275*, 24156–24162.

Kuhn, D.J., Chen, Q., Voorhees, P.M., Strader, J.S., Shenk, K.D., Sun, C.M., Demo, S.D., Bennett, M.K., van Leeuwen, F.W., Chanan-Khan, A.A., and Orlowski, R.Z. (2007). Potent activity of carfilzomib, a novel, irreversible inhibitor of the ubiquitin-proteasome pathway, against preclinical models of multiple myeloma. Blood *110*, 3281–3290.

Löwe, J., Stock, D., Jap, B., Zwickl, P., Baumeister, W., and Huber, R. (1995). Crystal structure of the 20S proteasome from the archaeon T. acidophilum at 3.4 A resolution. Science *268*, 533–539.

Martinez, C.K., and Monaco, J.J. (1991). Homology of proteasome subunits to a major histocompatibility complex-linked LMP gene. Nature *353*, 664–667.

Michalek, M.T., Grant, E.P., Gramm, C., Goldberg, A.L., and Rock, K.L. (1993). A role for the ubiquitin-dependent proteolytic pathway in MHC class I-restricted antigen presentation. Nature *363*, 552–554.

Muchamuel, T., Basler, M., Aujay, M.A., Suzuki, E., Kalim, K.W., Lauer, C., Sylvain, C., Ring, E.R., Shields, J., Jiang, J., et al. (2009). A selective inhibitor of the immunoproteasome subunit LMP7 blocks cytokine production and attenuates progression of experimental arthritis. Nat. Med. *15*, 781–787.

Murata, S., Sasaki, K., Kishimoto, T., Niwa, S., Hayashi, H., Takahama, Y., and Tanaka, K. (2007). Regulation of CD8+ T cell development by thymus-specific proteasomes. Science *316*, 1349–1353.

Nandi, D., Jiang, H., and Monaco, J.J. (1996). Identification of MECL-1 (LMP-10) as the third IFN-gamma-inducible proteasome subunit. J. Immunol. *156*, 2361–2364.

Nandi, D., Woodward, E., Ginsburg, D.B., and Monaco, J.J. (1997). Intermediates in the formation of mouse 20S proteasomes: implications for the assembly of precursor beta subunits. EMBO J. *16*, 5363–5375.

Nett, M., Gulder, T.A., Kale, A.J., Hughes, C.C., and Moore, B.S. (2009). Function-oriented biosynthesis of beta-lactone proteasome inhibitors in Salinispora tropica. J. Med. Chem. *52*, 6163–6167.

Orlowski, M., Cardozo, C., and Michaud, C. (1993). Evidence for the presence of five distinct proteolytic components in the pituitary multicatalytic proteinase complex. Properties of two components cleaving bonds on the carboxyl side of branched chain and small neutral amino acids. Biochemistry *32*, 1563–1572.

Potts, B.C., Albitar, M.X., Anderson, K.C., Baritaki, S., Berkers, C., Bonavida, B., Chandra, J., Chauhan, D., Cusack, J.C., Jr., Fenical, W., et al. (2011). Marizomib, a proteasome inhibitor for all seasons: preclinical profile and a framework for clinical trials. Curr. Cancer Drug Targets *11*, 254–284.

Puttaparthi, K., and Elliott, J.L. (2005). Non-neuronal induction of immunoproteasome subunits in an ALS model: possible mediation by cytokines. Exp. Neurol. *196*, 441–451.

Rammensee, H.G., Friede, T., and Stevanoviíc, S. (1995). MHC ligands and peptide motifs: first listing. Immunogenetics *41*, 178–228.

Rock, K.L., and Goldberg, A.L. (1999). Degradation of cell proteins and the generation of MHC class I-presented peptides. Annu. Rev. Immunol. *17*, 739–779.

Romero, P., Corradin, G., Luescher, I.F., and Maryanski, J.L. (1991). H-2Kd-restricted antigenic peptides share a simple binding motif. J. Exp. Med. *174*, 603–612.

Schmidtke, G., Emch, S., Groettrup, M., and Holzhutter, H.G. (2000). Evidence for the existence of a non-catalytic modifier site of peptide hydrolysis by the 20 S proteasome. J. Biol. Chem. *275*, 22056–22063.

Seifert, U., Bialy, L.P., Ebstein, F., Bech-Otschir, D., Voigt, A., Schröter, F., Prozorovski, T., Lange, N., Steffen, J., Rieger, M., et al. (2010). Immunoproteasomes preserve protein homeostasis upon interferon-induced oxidative stress. Cell *142*, 613–624.

Singh, A.V., Bandi, M., Aujay, M.A., Kirk, C.J., Hark, D.E., Raje, N., Chauhan, D., and Anderson, K.C. (2011). PR-924, a selective inhibitor of the immunoproteasome subunit LMP-7, blocks multiple myeloma cell growth both in vitro and in vivo. Br. J. Haematol. *152*, 155–163.

Toes, R.E., Nussbaum, A.K., Degermann, S., Schirle, M., Emmerich, N.P., Kraft, M., Laplace, C., Zwinderman, A., Dick, T.P., Müller, J., et al. (2001). Discrete cleavage motifs of constitutive and immunoproteasomes revealed by quantitative analysis of cleavage products. J. Exp. Med. *194*, 1–12.

Tomaru, U., Ishizu, A., Murata, S., Miyatake, Y., Suzuki, S., Takahashi, S., Kazamaki, T., Ohara, J., Baba, T., Iwasaki, S., et al. (2009). Exclusive expression of proteasome subunit beta5t in the human thymic cortex. Blood *113*, 5186–5191.

Townsend, A., Bastin, J., Gould, K., Brownlee, G., Andrew, M., Coupar, B., Boyle, D., Chan, S., and Smith, G. (1988). Defective presentation to class I-restricted cytotoxic T lymphocytes in vaccinia-infected cells is overcome by enhanced degradation of antigen. J. Exp. Med. *168*, 1211–1224.

Tu, L., Moriya, C., Imai, T., Ishida, H., Tetsutani, K., Duan, X., Murata, S., Tanaka, K., Shimokawa, C., Hisaeda, H., and Himeno, K. (2009). Critical role for the immunoproteasome subunit LMP7 in the resistance of mice to Toxoplasma gondii infection. Eur. J. Immunol. *39*, 3385–3394.

Unno, M., Mizushima, T., Morimoto, Y., Tomisugi, Y., Tanaka, K., Yasuoka, N., and Tsukihara, T. (2002). The structure of the mammalian 20S proteasome at 2.75 A resolution. Structure *10*, 609–618.

Van den Eynde, B.J., and Morel, S. (2001). Differential processing of class-I-restricted epitopes by the standard proteasome and the immunoproteasome. Curr. Opin. Immunol. *13*, 147–153.

van Endert, P. (2011). Providing ligands for MHC class I molecules. Cell. Mol. Life Sci. *68*, 1467–1469.

Van Kaer, L., Ashton-Rickardt, P.G., Eichelberger, M., Gaczynska, M., Nagashima, K., Rock, K.L., Goldberg, A.L., Doherty, P.C., and Tonegawa, S. (1994). Altered peptidase and viral-specific T cell response in LMP2 mutant mice. Immunity *1*, 533–541.

Visekruna, A., Slavova, N., Dullat, S., Gröne, J., Kroesen, A.J., Ritz, J.P., Buhr, H.J., and Steinhoff, U. (2009). Expression of catalytic proteasome subunits in the gut of patients with Crohn's disease. Int. J. Colorectal Dis. *24*, 1133–1139.

Yewdell, J., Lapham, C., Bacik, I., Spies, T., and Bennink, J. (1994). MHC-encoded proteasome subunits LMP2 and LMP7 are not required for efficient antigen presentation. J. Immunol. *152*, 1163–1170.